Science Press

ARTICLE

Microstructure and Elevated Temperature Mechanical Properties of Al$_2$O$_3$/TiB$_2$/Al Composites

Wang Jia[1,2],   Liu Wei[2],   Shu Guogang[3],   Li Qiulin[1]

[1] Tsinghua Shenzhen International Graduate School, Shenzhen 518055, China; [2] School of Materials Science and Engineering, Tsinghua University, Beijing 100084, China; [3] China Nuclear Power Engineering Co., Ltd, Shenzhen 518172, China

Abstract: Aluminum matrix composites with micro-TiB$_2$ and nano-Al$_2$O$_3$ particles were successfully fabricated by combining powder metallurgy and hot rolling using raw materials of fine atomized aluminum powders and TiB$_2$ particles. Results show that the Al$_2$O$_3$/TiB$_2$/Al composites exhibit a yield strength of 258.7 MPa and an ultimate tensile strength of 279.3 MPa at 25 °C due to the comprehensive strengthening effect of TiB$_2$ and Al$_2$O$_3$ particles. The strengthening effect of TiB$_2$ particles significantly weakens with rising the temperature to 350 °C, and the Orowan strengthening mechanism between nano-Al$_2$O$_3$ and dislocation makes the yield strength and tensile strength of the composite material reach 98.2 and 122.5 MPa, respectively. After annealing at 350 ℃ for 1000 h, due to the pinning effect of nano-Al$_2$O$_3$ at grain boundaries, the grains growth is suppressed significantly, and the strength and hardness do not decrease significantly.

Key words: TiB$_2$/Al composites; nano-Al$_2$O$_3$ particles; mechanical properties; thermal stability

Particle-reinforced aluminum matrix composites are widely used in the transportation, construction, military, aerospace, and nuclear industries due to their lightweight, excellent specific strength, good wear resistance, low coefficient of thermal expansion (CTE), and high heat conductivity compared to the properties of monolithic aluminum alloys[1-4]. Compared to the ceramic particles such as SiC, B$_4$C, Al$_2$O$_3$, and TiC, titanium diboride (TiB$_2$) exhibits outstanding properties such as high melting point (2790 °C), high hardness (HV=9600 MPa), high elastic modulus (550 GPa), and good thermal stability[1,5], and has become an attractive composition for aluminum matrix composites. Especially, TiB$_2$ phase does not react with aluminum, so TiB$_2$/Al composites have great potential for application in dry storage and transportation of spent fuel.

Materials absorbing thermal neutrons continuously may undergo a high-temperature environment (350 °C) for long periods[6]. So far, various aspects of TiB$_2$/Al composites have been studied, especially in term of their tensile properties[7,8], wear performance[9] and fatigue behavior[10] at room temperature. However, few researches about elevated

temperature tensile properties of TiB$_2$/Al composites were investigated. Yi et al[11] fabricated TiB$_2$/Al-Si composites by reaction processing method. The results show that the ultimate tensile strength (UTS) of composites is higher than that of Al-Si matrix at 25~400 °C. Oñoro[12] fabricated TiB$_2$/Al (6061 and 7015) composites by powder metallurgy (PM) and hot extrusion. The results show that the UTS of composites reduces quickly, due to the failure of aging strengthening of the matrix alloy by coarsening the precipitates at 200~300 °C. Han et al[2] studied in situ TiB$_2$/Al-12Si composites fabricated by exothermic reaction and obtained similar conclusions. Results show no noticeable improvement in the yield strength (YS) and UTS of the composites, compared with the properties of matrix alloy at 200~350 °C. The precipitate coarsening and fracture behavior of the composites transformed from particle cracking to particle-matrix interface debonding collectively contributes to the reduction of strength at elevated temperature.

Al matrix nanocomposites are widely studied to obtain excellent mechanical properties at elevated temperature. The recently developed in-situ nano-Al$_2$O$_3$ reinforced Al

matrix composites, namely high-temperature aluminum (HITEMAL)[13], possess superior tensile and thermal stability at elevated temperatures due to the unique strengthening of nano-Al_2O_3 distributed at high-angle grain boundaries (HAGBs). Balog et al[14] fabricated the bulk Al matrix composites reinforced with a nanometric amorphous Al_2O_3 (am-Al_2O_3) network by PM, which shows superior properties at elevated temperatures. The stability of grain boundaries (GBs) at 600 °C is attributed to the Zener drag of in-situ Al_2O_3. Besides, the fabrication of Al matrix nanocomposites reinforced with bimodal size distribution through the introduction of micro-sized and nano-sized reinforcement is an effective method. Gao et al[15] introduced the in-situ hybrid-sized TiC_x-TiB_2 with sizes ranging from 20 nm to 1.3 μm into Al-Cu-Mg-Si alloy. Results show that the composites exhibit the yield strength of 141 MPa, and tensile strength of 164 MPa, due to the grain boundary pinning effect by the hybrid-sized TiC_x-TiB_2 particles. Thus, the introduction of nanoparticles into the aluminum alloy matrix is a promising method to improve its elevated temperature performance. However, the acquirement of well dispersed nano particles by ex-situ approach is difficult. Poletti et al[16] concluded that the nano-Al_2O_3 particles can be introduced into the matrix by compacting fine atomized aluminum powders, and the processing parameters have great effect on the distribution and phase state of Al_2O_3, which is originated from the am-Al_2O_3 layer[17-19].

In the present work, Al_2O_3/TiB_2/Al composites were fabricated by powder metallurgy with raw materials of fine atomized aluminum powders and the microstructures were observed. Mechanical properties and thermal stability at elevated temperature were investigated. Fractographic analysis was conducted to examine the effect of temperature on fracture behavior.

1 Experiment

The commercially available pure aluminum powder with mean particle size of ~1.5 μm and titanium diboride (TiB_2) with mean particle size of ~6.8 μm, as shown in Fig.1, were used as raw materials. The chemical composition of aluminum powder is given in Table 1. The Al_2O_3 phase originated from the thin oxide film presents on the surface of the fine atomized aluminum powder[13,14,20]. The Al_2O_3/TiB_2/Al composites containing 16vol% TiB_2 particles were fabricated by powder metallurgy. The Al_2O_3/Al composites without TiB_2 particles were prepared for comparison. Both composites contained 3vol% Al_2O_3. Pure aluminum and TiB_2 powders were mixed in alcohol medium at 150 r/min for 1.5 h in the grinder (1-S Lab), and the mass ratio between the ball and mixed powder was 6:1. The mixed powder slurry was dried at 70 °C for 24 h, and then the large lumps were crushed by the pulverizer. The dried powders were placed in a mold with the size of Φ150 mm× 180 mm

and compacted by cold isostatic pressing (CIP) at 400 MPa for 2 min. The green compacts were sintered at 500 °C for 3 h under the vacuum degree of 2×10^{-3} Pa, removing the residual gas and free water of the atomized powder surface. Samples with a thickness of 10 mm were prepared for hot rolling at 590 °C. Finally, the sample was rolled to 3 mm through multiple passes with dwelling time of 30 min after each pass to eliminate internal stress during rolling.

Samples of sintered and rolled composites were mechanically polished with graded SiC emery paper, ranging from 400# to 1500#, followed by ion beam polishing (IB-09020CP, JEOL) at a voltage of 6 kV for 5 h. The phase composition of composites was identified by X-ray diffraction (XRD, DLMAX 2500) with Cu Kα radiation (λ=0.1542 nm) at a scanning speed of 5°/min. Raw powders and the microstructure of composites were observed by scanning electron microscope (SEM, Hitachi S4800). Samples for electron back-scattered diffraction (EBSD, TESCAN MIRA 3 LMH) analyses were observed with scan grid of 0.2 μm in step size. Moreover, samples were observed in detail by transmission electron microscope (TEM, FEI Tecnai G2 F30) at an accelerating voltage of 200 kV. The density of the composites was measured three times for each sample by the Archimedes method in distilled water. The theoretical density of Al_2O_3/TiB_2/Al and Al_2O_3/Al composites was estimated by the rule of mixtures using Eq.(1) and Eq.(2), respectively, with the theoretical density of 4.52[21], 2.71[14] and 3.66 g/cm3[22] for TiB_2, pure Al and γ-Al_2O_3 phase, respectively:

$$\rho_1 = \rho_{TiB_2} V_{TiB_2} + \rho_{Al} V_{Al} + \rho_{\gamma\text{-}Al_2O_3} V_{\gamma\text{-}Al_2O_3} \qquad (1)$$

$$\rho_2 = \rho_{Al} V_{Al} + \rho_{\gamma\text{-}Al_2O_3} V_{\gamma\text{-}Al_2O_3} \qquad (2)$$

Where V_{TiB_2}, V_{Al} and $V_{\gamma\text{-}Al_2O_3}$ represent the volume fraction of TiB_2, Al and γ-Al_2O_3, respectively.
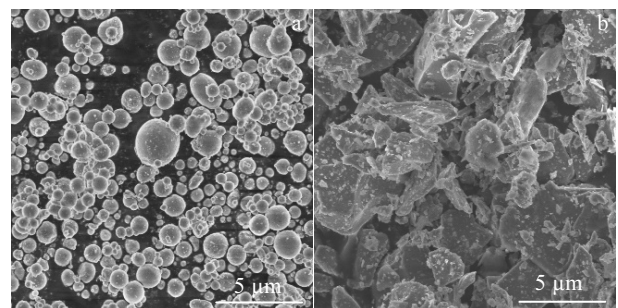
Hardness was measured at the polished section of the sam-

Fig.1   SEM morphologies of raw Al powders (a) and TiB_2 particles (b)

Table 1   Chemical composition of the aluminum powder (wt%)

Cu	Fe	Si	H	O	Al
≤0.015	≤0.2	≤0.2	≤0.003	≤0.028	Bal.

ples by a Vickers hardness tester (HVS-1000B) equipped with a pyramid indenter with the load of 300 N and dwelling time of 10 s. Each sample was tested 10 times to obtain the mean value. Tensile tests were carried out on the MTS Landmark testing system (MTS, Eden Prairie, MN, USA) equipped with a heating furnace at the strain rate of 1×10^{-3} s^{-1} and the test temperature range of 25~450 °C. Gradient heating was adopted to control the temperature in order to avoid exceeding the set temperature of the elevated temperature test. The final temperature error was controlled within ±1 °C. The soaking time was 5 min before the test. Rectangular specimens were machined for tensile tests, and repetitive tests were conducted to ensure the accuracy of results.

2 Results and Discussion

2.1 Microstructure

XRD pattern of the rolled $Al_2O_3/TiB_2/Al$ composites is shown in Fig.2. The XRD result shows that Al and TiB_2 phases are detected. However, the nano-Al_2O_3 phase is not found, and Al_2O_3 phase is identified in the following TEM analysis.

Fig.2 XRD pattern of $Al_2O_3/TiB_2/Al$ composites
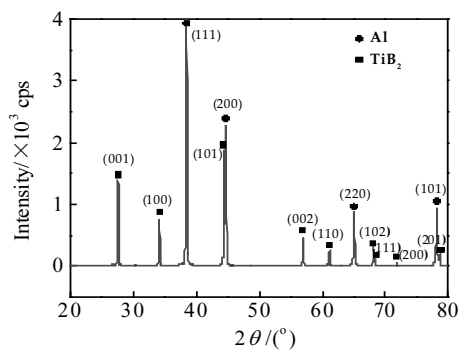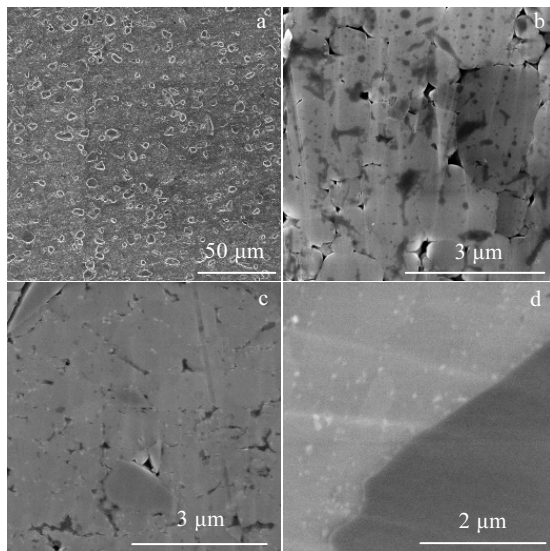

Fig.3 SEM images of $Al_2O_3/TiB_2/Al$ composites: (a) distribution of TiB_2 particles; (b, c) as-sintered and rolled composites with reduction ratio of 30%; (d) interface of composites with reduction ratio of 70%

Fig.3 shows the microstructure of $Al_2O_3/TiB_2/Al$ composites. In Fig.3a, uniform distribution of TiB_2 particles is observed in composites. Fig.3b~3d show the microstructure change of composites with the increase of reduction ratio. Micropores are clearly observed in the as-sintered samples (Fig.3b), which is consistent with its relative density of 94.7% (Table 2). As the reduction ratio increases, the quantity and size of micropores decreases (Fig.3c and 3d), and micropores almost disappear after rolling with the reduction ratio of 70% (Fig.3d). The measured relative density of rolled $Al_2O_3/TiB_2/Al$ and Al_2O_3/Al composites is about 99.4% and 99.6%, respectively, and is close to the theoretical density. Fig.4a shows the EBSD mapping result of $Al_2O_3/TiB_2/Al$ composites, and the average grain size of composites is (1.03±0.86) μm after the hot rolling deformation, as shown in Fig.4b.

Table 2 Relative density and hardness of as-sintered and rolled composites

Material	Relative density/%	Hardness, HV/MPa
As-sintered $Al_2O_3/TiB_2/Al$ composite	94.7	854
Rolled $Al_2O_3/TiB_2/Al$ composite	99.4	1127
Rolled Al_2O_3/Al composite	99.6	689

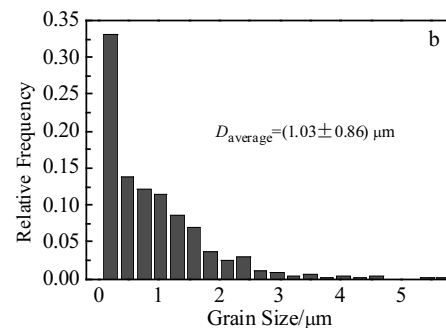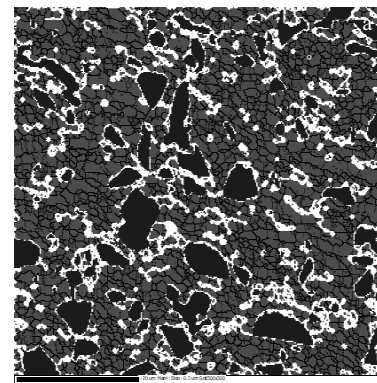
Fig.4 EBSD results for rolled $Al_2O_3/TiB_2/Al$ composites: (a) phase mapping of grain boundaries; (b) grain size distribution of $Al_2O_3/TiB_2/Al$ composites (red and blue in Fig.4a represent Al and TiB_2 phases, respectively)

2.2 TEM analyses

Research indicates that the native Al_2O_3 films on the fine atomized Al powders are amorphous[17,23] and the am-Al_2O_3 transforms to γ-Al_2O_3 when the temperature exceeds 450 °C[14]. Bright field TEM images of rolled Al_2O_3/TiB_2/Al composites are shown in Fig.5. It is found that the Al_2O_3 particles distributed in matrix are mainly located near GBs and the am-Al_2O_3 layers are difficult to observe (Fig.5a). High-resolution (HR) TEM images and corresponding fast Fourier transform (FFT) patterns captured in the Al_2O_3 phase provide evidence that this Al_2O_3 phase distributed near GBs is γ-Al_2O_3 with a face-centered cubic structure (Fig.5c and 5d). The average size of γ-Al_2O_3 particles is about (47±11) nm (~100 particles were measured). Fig.5b shows the microstructure that Al_2O_3 phase has irregular morphology. It is noteworthy that the interface between Al_2O_3 particles and Al matrix is clear and the materials are well combined in HRTEM images.

2.3 Mechanical properties of composites

Fig.6 shows the engineering stress-strain curves of composites at room temperature. It can be seen that the hot rolling deformation significantly improves the tensile strength and hardness of the Al_2O_3/TiB_2/Al composites (Fig.6 and Table 2). The UTS and hardness (HV) of Al_2O_3/TiB_2/Al composites increase from 107 MPa to 279.3 MPa and from 854 MPa to 1127 MPa, respectively. As shown in Fig. 6 and Table 2, the UTS and hardness (HV) of Al_2O_3/Al composite value reach 208.4 MPa and 689 MPa, and Al_2O_3/TiB_2/Al composites have 34% and 63.7% higher than the UTS and hardness value of Al_2O_3/Al composites

Fig.5   Bright field TEM images (a, b) and HRTEM image (c) of rolled Al_2O_3/TiB_2/Al composites; corresponding fast Fourier transform (FFT) pattern captured on γ-Al_2O_3 particles (d)

counterpart at room temperature. However, significant improvement in plasticity can be observed for Al_2O_3/Al composites.

Engineering stress-strain curves in Fig. 6 show that fracture always takes place before yielding for sintered composites. This phenomenon is consistent with the observation of microstructure exhibiting micropores and lower relative density. It is worth pointing out that the plasticity of composites improves via rolling deformation, but it is still low. This is similar to the research of Balog et al[14]. The composites annealed at 600 °C fractures prematurely prior to yielding, with an average ε of ~0.7%. It is suggested that the incomplete degassing of cold isostatic pressed bulk in vacuum sintering leads to the residual gas in sintered compacts, which entraps gas expanded during hot rolling (590 °C), resulting in the nano-sized pores and deteriorating the strength and plasticity.

Variations of strength and plasticity of Al_2O_3/TiB_2/Al composites as a function of test temperature are shown in Fig.7. As shown in Fig.7a, compared with the tensile curve at 25 °C, the plasticity of composites at 150~450 °C increases and the strength decreases. Fig.7b shows that both YS and UTS decrease linearly as the temperature increases. The UTS of composites is 122.5 MPa at 350 °C, and 83.9 MPa at 450 °C. For Al_2O_3/Al composites, the UTS is 100 MPa at 350 °C. Compared with the tensile increment at room temperature, the increment of UTS of the Al_2O_3/TiB_2/Al composites is less at 350 °C. UTS between Al_2O_3/TiB_2/Al and Al_2O_3/Al composites decreases from 70.9 MPa to 22.5 MPa when the test temperature rises from 25 °C to 350 °C, as listed in Table 3. At elevated temperature, the introduction of micro-TiB_2 particles into Al_2O_3/Al composites has no significant contribution to strength.

2.4 Thermal stability of mechanical properties at 350 °C

Neutron-absorbing materials for dry storage serve at 350 °C for a long time due to the continuous absorption of thermal neutrons[6]. In this research, thermal stability of
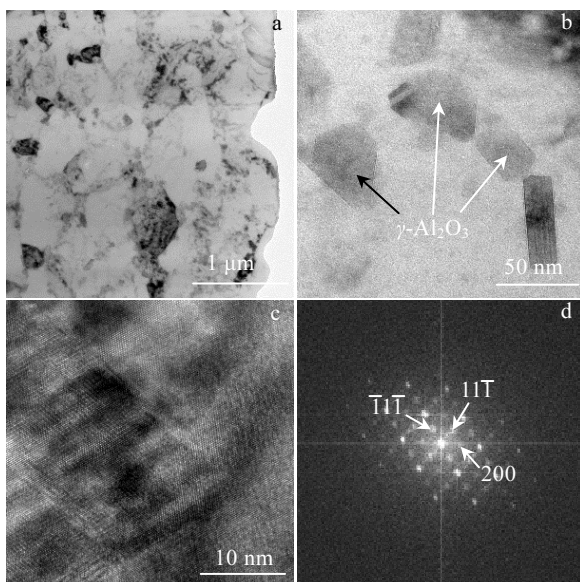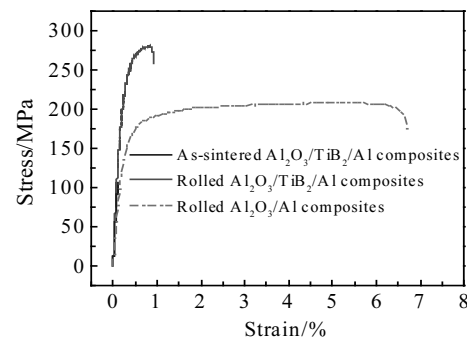

Fig.6   Engineering stress-strain curves of composites at room temperature

Table 3   UTS of rolled composites at 25 and 350 °C (MPa)

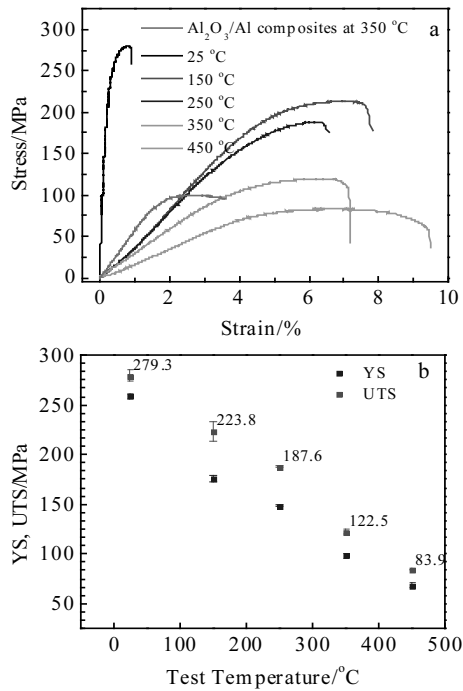| T/°C	$Al_2O_3/TiB_2/Al$ composite	Al_2O_3/Al composite	UTS
25	279.3	208.4	70.9
350	122.5	100	22.5

Fig.7   Tensile properties of $Al_2O_3/TiB_2/Al$ composites: (a) engineering stress-strain curves; (b) yield strength (YS) and ultimate tensile strength (UTS) as a function of test temperature

rolled $Al_2O_3/TiB_2/Al$ composites annealed at 200 °C for 2 h was evaluated by holding at 350 °C for 1000 h. Fig.8 shows the mechanical properties at 350 °C of composites including UTS, YS, and hardness as a function of soaking time. After processing for 1000 h, the UTS and YS curves fluctuate slightly and show no significant decrease, indicating no evident change of microstructure. It is worth pointing out that the tensile strength decreases from 279.3 MPa to 257.4 MPa after the treatment at 350 °C for 400 h. Due to incomplete annealing after rolling, the dislocation density decreases in the recovery process during heat treatment at 350 °C and the strength decreases correspondingly. The hardness curve is stable, and the hardness is unchanged after the 1000 h annealing process, which is consistent with the change trend of tensile strength.

It is well known that the strength of pure Al matrix can only be obtained by strain strengthening via deformation, and the grain grows slowly in the high-temperature environment, leading to the serious deterioration of mechanical properties. In this research, excellent thermal stability of $Al_2O_3/TiB_2/Al$ composites is acquired by introducing in-situ nano-Al_2O_3. Fig.5a and 5b show that the γ-Al_2O_3 nucleates near the Al-Al interface and grows epitaxially, and the interface between Al and Al_2O_3 is clear indicating the materials are well bonded. During the process of annealing at 350 °C for 1000 h, the γ-Al_2O_3 and TiB_2 ceramic phases show good thermal stability and the size, distribution and quantity of particles are unchanged. Thus, the nanoparticles effectively hinder the movement of GBs and the grain growth The EBSD results in Fig.9a also show that the grain growth is not observed, and the average grain size is 0.97 μm in Fig.9b. The Hall-Petch effect is still one of the main strengthening mechanisms. Therefore, the microstructure stability triggered by nano-γ-Al_2O_3 phase ensures the outstanding stability of mechanical properties at elevated temperatures.

2.5   Strengthening mechanism at room/elevated temperature

The effect of the introduction of hard micro-sized and nano-sized particles into the soft metallic matrices on the mechanical properties is well discussed. Strengthening models, such as Hall-Petch strengthening, load-bearing, mismatch of CTE and elastic modulus (EM) between the reinforcement and matrix, and Orowan strengthening, have been proposed during the past three decades, synthetically contributing to the tensile strength of composites[24,25]. In this work, micro-TiB_2 and nano-Al_2O_3 phases as reinforcement were introduced into the pure aluminum matrix and the main strengthening mechanisms are as follows.

(1) Hall-Petch strengthening

Mechanical properties of the composites are greatly influenced by the microstructure, especially by the grain size. Reinforcement can stimulate the initiation of dynamic recrystallization and the grain is refined[26]. During the processing of hot rolling deformation, the dynamic recrystallization is stimulated by the TiB_2 and Al_2O_3 particles and the grain of composites is refined, as shown in Fig.4a. The
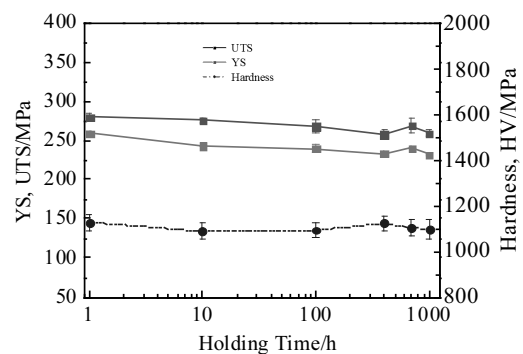

Fig.8   Mechanical properties of $Al_2O_3/TiB_2/Al$ composites as a function of processing time at 350 °C

strength calculated by Hall-Petch is expressed as follows[27]:

$$\sigma_{H\text{-}P} = \sigma_0 + \frac{k}{\sqrt{d}} \tag{3}$$

where σ_0 is the strength of Al matrix, k is the material constant with a value of ~2100 MPa·nm$^{1/2}$ and d is the grain size with a value of ~1.03 μm.

(2) Orowan strengthening

Orowan strengthening is the interaction between the second phase and dislocations. When the composites deform, dislocations encountering the hard second phase largely proliferate to produce dislocation rings, which improves the yield strength of the material. The strengthening mechanism of Orowan-Ashby equation[28,29] is shown as follows:

$$\Delta\sigma_{OR} = \frac{0.13bG_m}{d_p\left(\sqrt[3]{\frac{1}{2V_p}} - 1\right)}\ln\frac{d_p}{2b} \tag{4}$$

where b is the magnitude of the Burgers vector of dislocations in the Al matrix (~0.286 nm), G_m is the shear modulus of the matrix (~26.4 GPa), d_p is the grain size, and V_p is the volume fraction of reinforcements. With the increase of volume fraction and the decrease of the particle size of the reinforcements, the enhancement effect based on Orowan

Fig.9   EBSD results of Al$_2$O$_3$/TiB$_2$/Al composites annealed at 350 °C for 1000 h: (a) phase map of grain boundaries; (b) grain size distribution of Al$_2$O$_3$/TiB$_2$/Al composites (red and blue in Fig.9a represent Al and TiB$_2$, respectively)

mechanism on the YS of composites is more obvious. It is worth noting that Orowan strengthening is not the major factor when the size of reinforcements is ~5 μm or larger[24,28]. Therefore, the improved strength from the interaction between TiB$_2$ particles (~6.7 μm) and dislocations is lower in this research. Besides, in-situ nano-γ-Al$_2$O$_3$ can availably pin the dislocations, leading to tremendous promotion of mechanical properties of composites. Fig.10 shows that the strength increment by nano-Al$_2$O$_3$ is higher than that by TiB$_2$ particles.

(3) Mismatch of CTE and EM

Mismatch of the CTE and EM between reinforcement and matrix produces geometrically necessary dislocations (GNDs) during the cooling process of composite fabrication. The density of GNDs resulting from the mismatch of CTE and EM is calculated by Eq.(5) and Eq.(6)[29]:

$$\rho_{CTE} = \frac{A\Delta\alpha\Delta TV_p}{bd_p\left(1 - V_p\right)} \tag{5}$$

$$\rho_{EM} = \frac{6V_p}{\pi d_p^3}\varepsilon \tag{6}$$

where A is the geometrical constant with a value of ~12; $\Delta\alpha$ is the CTE difference between the matrix and particles; the α of Al, TiB$_2$ and Al$_2$O$_3$ phase is 24×10^{-6}, 8.1×10^{-6} and 7.7×10^{-6} K^{-1}, respectively; ΔT is the difference between processing temperature and test temperature. Thus, the increment of YS by mismatch of CTE and EM is acquired by the Taylor equation[30]:

$$\Delta\sigma_{CTE+EM} = \beta G_m b\left(\sqrt{\rho_{CTE}} + \sqrt{\rho_{EM}}\right) \tag{7}$$

where β is the constant with a value of ~1.25. The increase in GND with the decrease of particle size improves the YS of composites by Eq.(5) and Eq.(6). The calculation results indicate that GNDs of Al$_2$O$_3$ and TiB$_2$ particles offer the maximal contribution to the YS of composites.

(4) Load-bearing effect

The effective load transfers from soft matrix to non-shear particles through interface under applied external stress. A modified shear lag model proposed by Nardone and Prewo[31] is widely used to predict the strength contribution[28]:

$$\Delta\sigma_{L\text{-}T} = 0.5V_p\sigma_m \tag{8}$$

where σ_m is the YS of unreinforced matrix. The bearing capacity of reinforcements becomes stronger with the increase of their volume fraction. Nano-Al$_2$O$_3$ particles with volume fraction of less than 3vol% are not the main bearing phase. 16vol% TiB$_2$ particles can offer efficient load transfer. The calculation results are also consistent with the results (Fig.10).

Fig.10 shows the calculation results of each strengthening mechanism and theoretical values of composites. Great
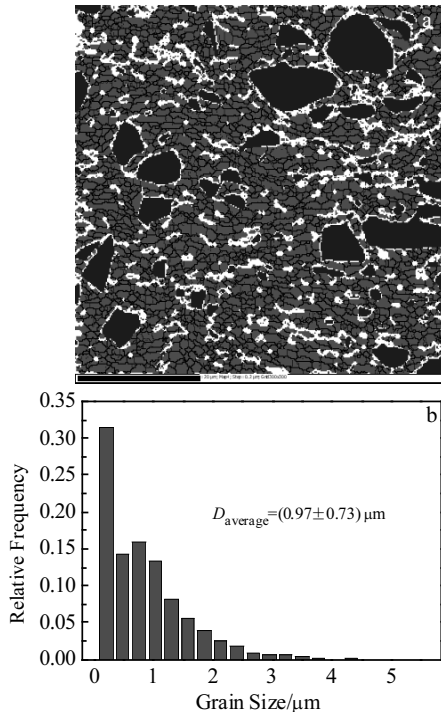
agreement between the experimental and predicted values is found for $Al_2O_3/TiB_2/Al$ composites. The small differences between theoretical and experiment values may be due to the interface defects, a few clusters of reinforcements, and the estimation error of the formula parameters.

Because materials used as a neutron-absorber medium undergo a long period at 350 °C, composites need excellent high-temperature strength and thermal stability. Fig.7b shows that the YS of composites linearly decreases as the temperature increases. From the results, the YS of $Al_2O_3/TiB_2/Al$ composites at 350 °C decreases to 122.5 MPa, which indicates that some of the strengthening mechanisms are effective and some fail at elevated temperatures. Tensile results in Fig.6 and 7 show that the difference of UTS between $Al_2O_3/TiB_2/Al$ and Al_2O_3/Al composites decreases as the test temperature increases, indicating that the enhancement effect of micro-TiB_2 particles greatly weakens at elevated temperature. Thus, the strength contribution by micro-TiB_2 particles is not considered at elevated temperature. Low matrix shear modulus values and weak bonding between the matrix and reinforcements are well known at high temperature[28]. Therefore, for nano-Al_2O_3, the mismatch of CTE and EM is also not an important strengthening mechanism at elevated temperature, compared with the properties at room temperature. Moreover, the lower interface bonding strength caused by increasing temperature makes the load-bearing effect unapparent.

Considering the microstructure, refinement strengthening and Orowan strengthening can explain the improved strength at 350 °C. First, refinement strength is related to the grain size, and grain growth at elevated temperature deteriorates the tensile strength due to the increase of grain-boundary activation energy[32]. TEM analysis shows that the efficiency of GBs is enhanced by nano-γ-Al_2O_3 particles

distributed at the GBs. The EBSD result of composites annealed at 350 °C for 1000 h in Fig.9a also indicates that nano-Al_2O_3 particles effectively pin the GBs. Thus, Hall-Petch strengthening is still one of the main strengthening mechanisms at 350 °C. Secondly, metal matrix nanocomposites reinforced by nanoparticles are gradually employed in applications at high temperatures[26] because of the high thermal stability of ceramic nanoparticles by Orowan strengthening, which is one of the main mechanisms. During the deformation, nano-Al_2O_3 particles act as obstacles of dislocation motion, and the dislocations piling up around the particles improve the elevated temperature strength.

3 Conclusions

1) Microstructure analysis indicates that the TiB_2 particles are distributed uniformly in the Al matrix by the milling and hot rolling. In-situ nano-γ-Al_2O_3 particles are located near the grain boundaries and exhibit a mean size of (47 ± 11) nm.

2) The tensile strength of $Al_2O_3/TiB_2/Al$ composites decreases linearly as the temperature increases. At 350 °C, the composites exhibit yield strength of 98.2 MPa and ultimate tensile strength of 122.5 MPa.

3) Because the nano-Al_2O_3 particles hinder the motion of grain boundaries, the ultimate tensile strength, yield strength, and hardness of $Al_2O_3/TiB_2/Al$ composites are nearly unchanged after annealing at 350 °C for 1000 h.

References

1 Suresh S, Shenbag N, Moorthi V. *Procedia Engineering*[J], 2012, 38: 89

2 Han G, Zhang W, Zhang G *et al. Materials Science and Engineering A*[J], 2015, 633: 161

3 Zhang L, Shi J, Shen C *et al. Applied Sciences*[J], 2017, 7: 1009

4 Qin J, Zhang Z, Chen X G. *Journal of Composite Materials*[J], 2016, 51(18): 2643

5 Li H, Zhao S, Ou Y *et al. Science and Engineering of Composite Materials*[J], 2018, 25(3): 453

6 Lai J, Zhang Z, Chen X G. *Materials Science and Engineering A*[J], 2012, 532: 462

7 Sadeghian Z, Lotfi B, Enayati M H *et al. Journal of Alloys and Compounds*[J], 2011, 509(29): 7758

8 Wang T, Chen Z, Zheng Y *et al. Materials Science and Engineering A*[J], 2014, 605: 22

9 Chi H, Jiang L, Chen G *et al. Wear*[J], 2016, 368: 304

10 Wang F, Xu J, Li J *et al. Materials & Design*[J], 2012, 33: 236

11 Yi H, Ma N, Li X *et al. Materials Science and Engineering A*[J], 2006, 419(1): 12
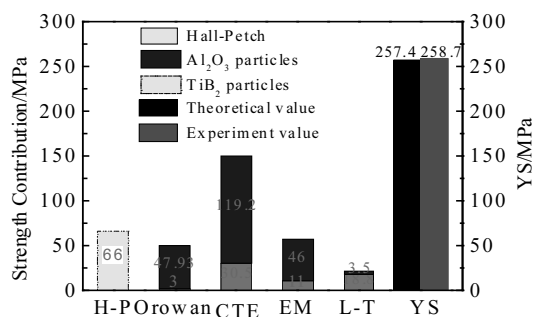
12 Oñoro J. *Rare Metals*[J], 2011, 30(2): 200

Fig.10 Measured and calculated strengthening contribution of micro-TiB_2 and nano-Al_2O_3 particles to the strength of $Al_2O_3/TiB_2/Al$ composites (H-P: Hall-Petch; CTE: coefficient of thermal expansion; EM: elastic modulus; L-T: load transfer)

13 Balog M, Simancik F, Bajana O *et al. Materials Science and Engineering A*[J], 2009, 504(1): 7

14 Balog M, Hu T, Krizik P *et al. Materials Science and Engineering A*[J], 2015, 648: 61

15 Gao Y Y, Dong B X, Qiu F *et al. Materials Science and Engineering A*[J], 2018, 728: 157

16 Poletti C, Balog M, Simancik F *et al. Acta Materialia*[J], 2010, 58(10): 3781

17 Rufino B, Boulc'h F, Coulet M V *et al. Acta Materialia*[J], 2007, 55(8): 2815

18 Balog M, Simancik F, Walcher M *et al. Materials Science and Engineering A*[J], 2011, 529: 131

19 Trunov M A, Schoenitz M, Zhu X *et al. Combustion and Flame*[J], 2005, 140(4): 310

20 Feng S Y, Li Q L, Liu W *et al. Rare Metals*[J], 2020, 39: 671

21 Chandana A, Lawrence I D, Jayabal S. *Materials Today: Proceedings*[J], 2018, 5(6): 14317

22 Balog M, Krizik P, Bajana O *et al. Journal of Alloys and Compounds*[J], 2019, 772: 472

23 Balog M, Poletti C, Simancik F *et al. Journal of Alloys and Compounds*[J], 2011, 509: S235

24 Luo G, Wu J, Xiong S *et al. Journal of Alloys and Compounds*[J], 2017, 701: 554

25 Alihosseini H, Dehghani K, Kamali J. *Advanced Powder Technology*[J], 2017, 28(9): 2126

26 Yang Q, Cheng DL, Liu J *et al. Materials Characterization*[J], 2019, 155: 109 834

27 Maung K, Earthman J C, Mohamed F A. *Acta Materialia*[J], 2012, 60(16): 5850

28 Zhang Z, Chen D L. *Materials Science and Engineering A*[J], 2008, 483: 148

29 Tang F, Anderson I E, Gnaupel-Herold T *et al. Materials Science and Engineering A*[J], 2004, 383(2): 362

30 Casati R, Vedani M. *Metals*[J], 2014, 4(1): 65

31 Nardone V C, Prewo K M. *Scripta Metallurgica*[J], 1986, 20(1): 43

32 Yang Y, Chen Y D, Hu H B *et al. Journal of Materials Research*[J], 2015, 30(22): 3502

Al$_2$O$_3$/TiB$_2$/Al 复合材料的微观结构和高温力学性能

汪 佳 [1,2]，刘 伟 [2]，束国刚 [3]，李丘林 [1]

(1. 清华大学深圳国际研究生院，广东 深圳 518055)

(2. 清华大学 材料学院，北京 100084)

(3. 中广核工程有限公司，广东 深圳 518172)

摘 要：以细雾化铝粉和 TiB$_2$ 颗粒为原料，通过粉末冶金和热轧制备微米 TiB$_2$ 和纳米 Al$_2$O$_3$ 颗粒增强铝基复合材料。室温时，由于 TiB$_2$ 和 Al$_2$O$_3$ 的综合强化作用，Al$_2$O$_3$/TiB$_2$/Al 复合材料的屈服强度和抗拉强度分别为 258.7 MPa 和 279.3 MPa，测试温度升至 350 ℃时，TiB$_2$ 颗粒的增强效果显著减弱，原位纳米 Al$_2$O$_3$ 颗粒与位错的交互作用使得复合材料的屈服强度和抗拉强度达到 98.2 MPa 和 122.5 MPa。经 350 ℃退火 1000 h 后，由于纳米 Al$_2$O$_3$ 对晶界的钉扎作用抑制晶粒长大，强度和硬度未发生显著的降低。

关键词：TiB$_2$/Al复合材料；纳米Al$_2$O$_3$；力学性能；高温稳定性

作者简介：汪 佳，男，1994 年生，硕士，清华大学深圳国际研究生院，广东 深圳 518055，电话：0755-26036032，E-mail: wangjia17@mails.tsinghua.edu.cn